Design of a Wireless Charging System for e-Scooter

Jakub Skorvaga, Michal Frivaldsky*, Miroslav Pavelek
Department of Mechatronics and Electronics, FEIT, University of Zilina,
Univerzitna 8215/1, Zilina, Slovakia
michal.frivaldsky@feit.uniza.sk.com

***Abstract*—This article deals with the design and practical evaluation of a wireless charging system for e-scooters. As wireless charging undertakes popularity, initially, the state of the art within application area is realized. Consequently, due to variability of the configuration of the whole system, several alternatives are discussed considering the utilization of the power converter stages. High attention is given to the construction of the coupling elements and calculation of the main circuit components of the considered power converters. The experimental part of the paper is supported by the measurements of key properties, i.e., the operational characteristics of the whole converter system together with coupling coils. Here, the efficiency characteristics, together with the output power characteristics in dependency on the mutual distance between the transmitting and receiving coils, are evaluated. Received results represent an adequate design approach and practical use of the proposed Wireless Power Transfer (WPT) e-scooter charging configuration.**

***Index Terms*—Wireless power charging; Efficiency; Power converter; Transfer characteristic; Transfer distance.**

I. INTRODUCTION

The mode of transport by means of electric scooters and bicycles, currently an excessive number of motor vehicles on the roads, is finding increasing justification. This mode of transport brings with it many benefits, such as a reduction in urban emissions and a reduction in the number of motor vehicles, which has a positive effect on the flow of road traffic.

The increasing number of electric scooters and bicycles brings higher safety requirements. Today, most common electric scooters and bicycles are charged using conventional cable chargers. For this reason, they must be equipped with connectors for connecting the charger. Many problems arise with the use of connectors, such as oxidation sensitivity, low water resistance, and low versatility or compatibility. The wireless method of charging said electric vehicles represents a possible alternative to prevent potential technical problems [1]. In many articles, contemporary authors describe ways to optimize wireless power transfer systems [7]–[13].

Most research in the field of wireless electricity transfer has so far focused on the field of electric vehicle charging. Recently, however, we have registered an increased interest in the research and application of wireless transfer for smaller vehicles, such as electric scooters or bicycles [3]–[6].

Many challenges need to be overcome to implement the idea of wireless vehicle charging and put it into practice. Such challenges are, first and foremost, ensuring safety and minimizing the electromagnetic field around the charging system, which can have a negative impact on the human body. Another hurdle that needs to be overcome is the choice of the optimal topology of power electronic circuits to ensure stable operation and maximize efficiency. Furthermore, it is necessary to develop algorithms for optimal control and implementation of communication between the charging station and the electric scooter. The spatial arrangement of the system, the external design, the implementation of the coupling elements of the wireless transfer to the scooter, and the demands on compactness must also be considered in the final design.

The power levels of charging systems for e-scooters and bicycles in the professional literature range from 100 W to 500 W. However, in most of the literature sources, the discussion is limited to systems that do not provide more than 200 W of power [1]. In [4], the authors presented a design of 100 W E-bike battery charger, which has also been tested in laboratory conditions. The authors in [1] described the design and laboratory measurement of an E-bike charging system capable of transmitting a power of 500 W with an efficiency higher than 90 %.

This article describes the design and construction of a wireless charging system (WChS) with a nominal charging power of 200 W for e-scooters. Initially, the selection of a suitable power semiconductor system concept is discussed. Consequently, based on known input/output parameters, the main part of the paper describes the design, Finite element method (FEM) simulation, and fabrication of coupling elements with respect to the dimensions of the scooter. Experimental part is focused on the evaluation of individual power electronic systems implemented together with a compensation network and coupling system to identify the operational characteristics of the proposed WChS for e-scooter. Here, the efficiency and power transfer

Manuscript received 9 December, 2020; accepted 1 April, 2021.

This publication was realized with the support of the Operational Program Integrated Infrastructure 2014–2020 of the project "Innovative Solutions for Propulsion, Power and Safety Components of Transport Vehicles", Grant No. ITMS 313011V334, co-financed by the European Regional Development Fund. The research was also supported by the National Grant Agency (APVV) under Grant. No. APVV – 0345-17.

characteristics are determined for several values of transmitting distances.

II. STATE OF THE ART WITHIN E-SCOOTER CHARGERS

To determine the parameters of the proposed e-scooter WChS, it was necessary to perform a survey of the parameters of the most commercially available electric scooter chargers on the market. Table I lists some types of e-scooter chargers, along with their basic parameters.

From the data given in Table I, we can see that the output voltage of commercial chargers for e-scooters ranges from 24 V to 52 V. The output voltage for the proposed solution was defined to 42 V and the nominal output power to 200 W. The higher value of charging power is related to the possibilities of fast charging.

TABLE I. OVERVIEW OF E-SCOOTER CHARGERS.

Type	Output voltage [V]	Output current [A]	Output power [W]
Xiaomi (clone)	42	2	85
iMeshbean	24	2	48
City Boss T7	52	2	104
Xiaomi MI	42	1.7	71.4

– Power Electronics Concept for Proposed e-Scooter WChS

Within this part of the paper, the description of the possible power electronic concept is being evaluated, indicating the advantages and disadvantages of individual solutions. Determination criterion for selection of the optimal configuration undertakes three different variants. Considering the practical implementation where international standards must be met, each solution is equipped with a power factor correction circuit to reduce negative impacts on the supply grid.

The 1st variant shown in Fig. 1 considers with the primary side arranged as standard power supply units, i.e., a grid rectifier followed by the Power Factor Correction (PFC) supplied by a 400 Vdc primary high-frequency (hf) inverter, primary coupling coil, and compensation network. The primary side represents the power electronic system located out of the e-scooter assembly. Secondary side (e-scooter parts) is composed of a coupling coil with the compensation network, the secondary side "hf" Schottky rectifier followed by DC/DC buck converter operated at CV/CC charging mode required by batteries.

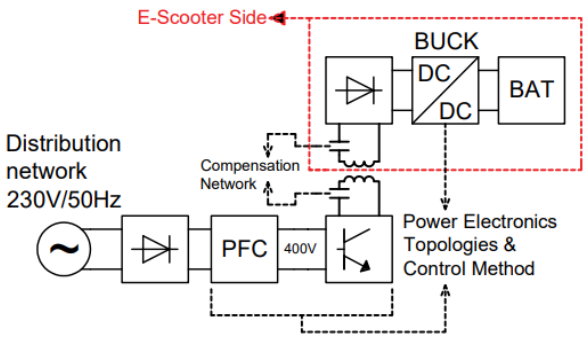

Fig. 1. First concept of power electronics arrangement for e-scooter WChS.

The disadvantage of the 1st concept lies in several operational principles. First, the power is being transferred by means of high voltage on the primary side, what results in large voltage stress on the compensation network (several kV). This is also the case of the secondary side coupling coil and compensation network (high voltage in close contact to the user). Secondarily, high voltage is reflected on the secondary side rectifier what puts higher requirements on the diodes (not standard, but high voltage SiC structures are required) and thus on the cost of the solution. The last negative drawback is reflected within the requirement on the wide voltage regulation of the DC/DC buck converter, where approximately 400 Vdc must be regulated down to 48 Vdc in CV/CC mode.

The possible way to eliminate the disadvantages related to high voltage stress is to put DC/DC buck converter on the primary side, i.e., between PFC and "hf" inverter (Fig. 2). This 2nd variant is not characterized by increased voltage stress on the compensation capacitors. Here, we propose to 400 Vdc/70 Vdc buck converter on the primary side operated in CV mode. On the secondary side, the utilization of an active synchronous rectifier operated at CV/CC mode is proposed for 2nd alternative. Using the concept presented in Fig. 2, the elimination of high voltage stress within the circuit components is possible.

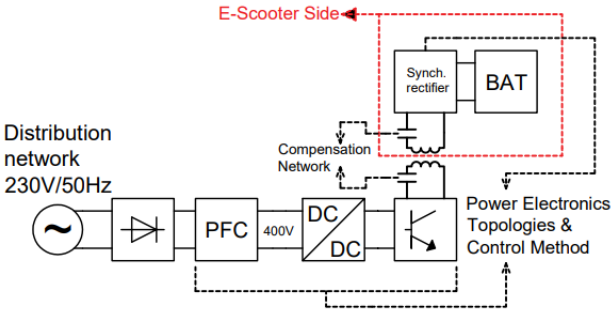

Fig. 2. Second concept of power electronics arrangement for e-scooter WChS.

However, the solution (Fig. 2) represents still some disadvantages related to the use of a secondary side synchronous rectifier, whose control within a wide operating range can be a complex task. Therefore, another concept is proposed.

The 3rd variant shown in Fig. 3 represents a combination of the previous two variants. The wireless transfer is realized here with reduced voltage as in the 2nd variant, while the secondary side uses a high-frequency low voltage Schottky rectifier followed by a buck type of DC/DC converter operated within CV/CC charging mode as valid for the 1st concept.

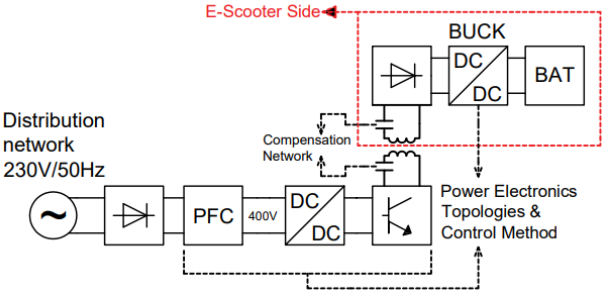

Fig. 3. Third concept of power electronics arrangement for e-scooter WChS.

The last presented solution combines the advantages of both previous concepts and simultaneously eliminates all disadvantages. The main negative drawback could be the reduced system efficiency compared to the 2nd concept.

The summary of the comparison of individual concepts is listed in Table II.

TABLE II. COMPARISON OF TOPOLOGY VARIANTS.

Critical properties	Variant_1	Variant_2	Variant_3
Safety	Low	Satisfactory	Satisfactory
Number of subsystems	6	6	7
Voltage stress of capacitors	High	Low	Low
Complexity of control algorithm	Medium	High	Medium
Cost	Very high	Satisfactory	Satisfactory
Efficiency	Medium	High	Medium

The advantages of the 1st concept lie in the simple control and low number of individual subsystems. Its main disadvantage is the high voltage stresses within the main circuit. The 2nd concept also contains a low number of individual subsystems, while reduced voltage is applied within WChS, reflecting as advantageous in terms of safety, efficiency, and reliability of the system. However, disadvantage is the complexity of the control algorithm of the secondary side synchronous rectifier. The 3rd concept, compared to the 2nd, contains up to seven subsystems, which makes it a more complex system in terms of components and has lower efficiency. However, on the other side, the charging control algorithm is much simpler. In terms of safety requirements, stable operation, and simplicity of the solution, the 3rd concept will be further investigated.

III. DESIGN OF COMPENSATION CIRCUIT AND COUPLING COILS

For charging systems, a suitable configuration of the compensation circuit is the use of series connection (Fig. 4) of capacitors both on the primary and secondary side [2]. When an electric field with a suitable resonant frequency is applied, the impedances of the capacitors and the coils cancel each other, thus ideally ensuring a zero-phase shift relative to the current flowing through the primary or secondary sides.

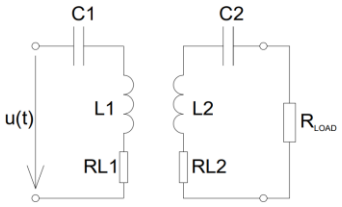

Fig. 4. Equivalent circuit for series compensation of wireless coupling system.

To determine the values of the inductances of the coupling coils, as well as the values of compensation capacitors, the already developed and optimized design procedure implemented as a software tool was used [2]. The input specifications for the proposed WChS are listed in Table III. Using the developed design procedure, it is initially required to define the six most important parameters. Based on these specifications, the automated calculations evaluate the required parameters of the coupling coils.

TABLE III. OVERVIEW OF INPUT PARAMETERS.

Output power [W]	200
Load resistance value [Ω]	10
Coil outer diameter [mm]	200
Transmission efficiency (coil-coil) [-]	0.98
Transmission distance [m]	0.1
Nominal frequency [kHz]	85

The diameter of the coil was determined to be 200 mm based on the dimensions of the base of the most commercially available e-scooters (Fig. 5). Considering the height of the e-scooter, the maximum power transfer distance is around 100 mm. According to the international standards [2], 85 kHz as the resonant frequency of the system was defined.

Table IV is listing the calculated parameters for the coupling coils. The diameter of the litz wire from which the coils are realized is 2 mm using 330 conductors. The radial spacing between individual turns is 4 mm. Because the number of turns is sufficient within one layer geometry, the axial turn displacement is 0. The inner diameter of the coil is set at 20 mm, while the coil should consist of 17 turns. The design procedure also defines the minimal amplitude of the input voltage (56 V) for the system to meet the required input/output parameters.

TABLE IV. OVERVIEW OF SOFTWARE OUTPUT FOR DESIGN.

Litz Wire diameter [mm]	2
Number of conductors [-]	330
Gap between turn axes [mm]	4
Axial gap between turns [mm]	0
Inner coil diameter [mm]	20
Number of turns [-]	17
Input voltage [V]	56

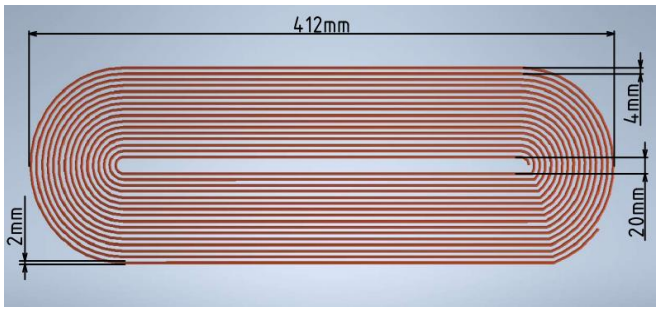

Fig. 5. Geometric model of the coil.

Developed software tool is provides also other important characteristics related to the coupling coil design. Figure 6 shows dependency of the coupling coefficient on the mutual distance between couplers. Listed here are also values of the compensation network itself, as well as the values of the parasitic resistances, which have been calculated based on the parameters of the coils (Table V).

TABLE V. OVERVIEW OF COUPLING CIRCUIT PARAMETERS.

Primary coil inductance [uH]	69.2
Secondary coil inductance [uH]	69.2
Primary capacitor capacity [nF]	50.67
Secondary capacitor capacity [nF]	50.67
Primary coil parasitic resistance [Ω]	0.0567
Secondary coil parasitic resistance [Ω]	0.0567

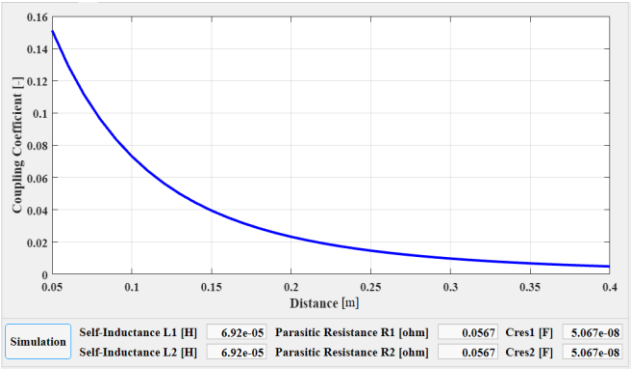

Fig. 6. Dependence of the coupling coefficient on the mutual distance.

The FEM model of the coupling elements as a product of the previous design is shown in Fig. 7 and can be used for the evaluation of the EM field radiation, or for the design of the magnetic shielding system if required.

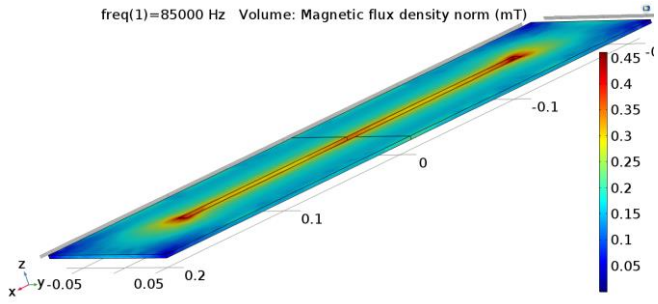

Fig. 7. FEM model of the designed coupling coils (without magnetic shielding).

Figure 8 shows the simulation results of the magnetic field radiation within the system of the proposed coupling coils (compensation network is considered as well). Here the distance between the receiver and transmitter was set to 0.1 m, while the nominal power, i.e., 200 W of the output power is transmitted. The EM field is symmetrically radiated from the primary coil, while the maximum of magnetic induction reaches 10 mT located at the top surface of this transmitter. According to ICNIRP 2010, the peak value of magnetic induction around the system of coils must be below 25 μT.

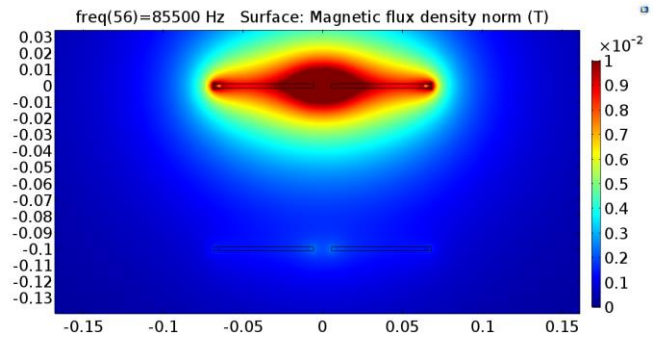

Fig. 8. Model of radiation of the system without shielding.

Therefore, it is necessary to supplement the coils with ferrite shielding in terms of prescribed hygiene standards (Fig. 9).

Integration of shielding increases the inductance of the coil and at the same time reduces the level of electromagnetic radiation to the system environment. Simulation tool calculates the value of shielded coil inductances with the value of 90.784 μH. Looking at the simulation results of the electromagnetic field radiation (Fig. 10), it is seen that most of the part of the radiated field from the top surface of the transmitting coil is significantly reduced.

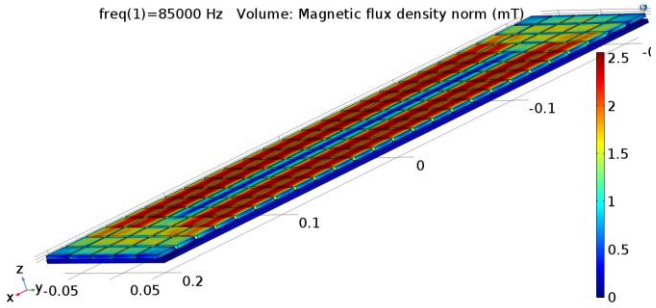

Fig. 9. FEM model of the designed coupling coils (with magnetic shielding).

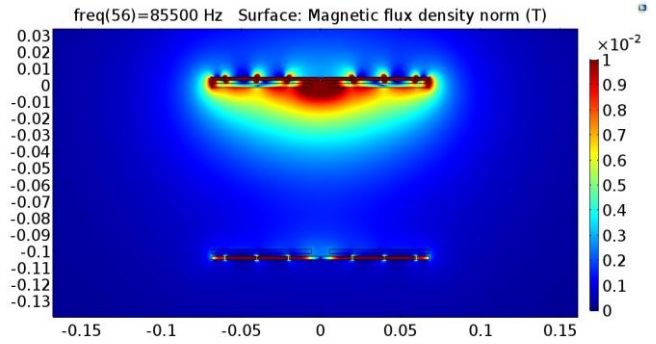

Fig. 10. Rectangular coil model with shielding.

With ferrite shielding applied using the Thomson relationship, the recalculated value of the compensation capacitance is 38.618 nF. With this combination, the quality factor of the resonant circuit Q reached a value of 16.1, what is more than 5 times higher compared to the coupling system without shielding.

IV. Construction of Experimental Model

A. Practical Implementation of Coupling Circuits

After the determination of the values of the key parameters of the coupling and compensation elements through calculation and simulation approach, a practical implementation of the functional model of the coils and capacitors is followed. The three-dimensional model of the coil's bobbin was designed in the Fusion 360 program according to the simulated parameters from the previous section. Prototype was made using a 3D printer and consequently assembled by conductor and ferrite shielding (Fig. 11). The physical model, therefore, contains both on the bottom and on the top part 120 folders for the application of shielding ferrite tablets with dimensions of 25 mm × 15 mm (Fig. 12).

The model of the coil is also equipped with connection ports for compensation capacitors (Fig. 11).

After fabrication, the inductance of the coil was measured to be 91.3 μH. Following the substitution of this value into the Tomson relationship, the capacitance value of the compensation capacitors was set to 38.4 nF to reach the resonant frequency of 85 kHz. For the realization of the

compensation capacitor, capacitors with a voltage rating of 400 V and a C0G dielectric have been used. The value of capacitance of one capacitor was 5.6 nF, thus fourteen pairs connected in parallel have been assembled, obtaining a total capacitance of 39.2 nF and a voltage rating of 800 V.

Fig. 11. Experimental model of a proposed coupling coil.

Fig. 12. Compensating capacitor.

B. *Experimental Prototypes of Power Electronic System*

For the practical realization of power electronic converters, the main circuit parameters have been evaluated to have an overview about the requirements for which circuit components they must be designed. Here it must be mentioned that according to the evaluation of the operation of individual converter stages, the microprocessor was used independently for each of the converters. The complete wireless charging system should be controlled by only one supervising microprocessor controller.

Power Factor corrector. The circuit schematic for the considered solution of PFC within the proposed e-scooter WChS is shown in Fig. 13. It consists of a standard bridge rectifier and a boost converter operated in PFC mode, while the core controller here is TMS 320F228069M. The main circuit variables required for the selection of circuit components are given by (1)–(6).

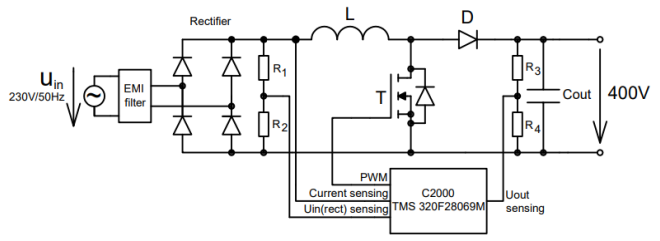

Fig. 13. Circuit diagram of the proposed PFC stage.

The average value of the input current flowing through the bridge rectifier is determined by (1), where P_o is the output power of PFC, $U_{AC(min)}$ is the minimal value of grid voltage

$$I_{AV} = \frac{2}{\pi} \times \frac{\sqrt{2} \times P_O}{U_{AC(\min)}} = \frac{2}{\pi} \times \frac{\sqrt{2} \times 250}{207} = 1,087A. \quad (1)$$

The value of inductance of PFC stage is given by (2)

$$L = \frac{1}{\%_{Ripple}} \times \frac{U_{AC(\min)}{}^2}{P_O} \times \left(1 - \frac{\sqrt{2} \times U_{AC(\min)}}{U_{out}}\right) \times$$
$$\times T_{SW} = \frac{1}{0,25} \times \frac{207^2}{250} \times \left(1 - \frac{\sqrt{2} \times 207}{400}\right) \times$$
$$\times \frac{1}{100 \times 10^3} = 1,838mH, \quad (2)$$

where $\%_{Ripple}$ is the current ripple of the coil and U_{out} is the output voltage of the PFC.

The values of the currents of the inductor, transistor, diode, and output capacitor are evaluated using (3)–(6):

$$I_{L(RMS)} = \frac{P_0}{U_{AC(\min)}} = \frac{250}{207} = 1,208A, \quad (3)$$

$$I_{AV} = \frac{2}{\pi} \times \frac{\sqrt{2} \times 250}{207} = 1,087A, \quad (4)$$

$$I_{D(AV)} = \frac{P_O}{U_{OUT}} = \frac{250}{400} = 0,625A, \quad (5)$$

$$I_{C(RMS)} = \sqrt{\frac{8 \times \sqrt{2} \times P_O{}^2}{3 \times \pi \times U_{AC(\min)} \times U_{OUT}} - \frac{P_O{}^2}{U_{OUT}{}^2}} =$$
$$= \sqrt{\frac{8 \times \sqrt{2} \times 250^2}{3 \times \pi \times 207 \times 400} - \frac{250^2}{400^2}} = 0,718A. \quad (6)$$

The selected main circuit components of the PFC stage are listed in Table VI.

TABLE VI. LIST OF USED CIRCUIT COMPONENTS OF THE PROPOSED PFC.

Component	Type/SN
Control circuit	TMS 320
Input rectifier module	GBU4J
PFC power inductor [mH]	1.838
Power transistor	IPA50R250
Power diode	MUR550
Output capacitor [uF]	220

Primary side DC/DC buck converter. Principal schematic for the primary side DC/DC buck converter in Fig. 14 is represented by a synchronous configuration, while the core control IC here is TMS 320F228069M.

The value of inductance of buck converter is given by (7)

$$L = \frac{U_{in(max)} - U_{OUT}}{\Delta I_L} \times t_{on(min)} =$$

$$= \frac{450-70}{0,857} \times 1,587 \times 10^{-6} = 703,7 \times 10^{-6} H, \qquad (7)$$

where ΔI_L is the current ripple of the coil and U_{OUT} is the output voltage of the buck converter, while $U_{in(max)}$ is the input voltage.

The selected main circuit components of the buck converter stage are listed in Table VII.

TABLE VII. LIST OF USED CIRCUIT COMPONENTS OF PROPOSED BUCK CONVERTER.

Component	Type/SN
Control circuit	TMS 320
Power inductor [uF]	703.7
Power transistor H	IPP60R360P7
Power transistor L	IPP60R360P7
Output capacitor [uF]	220

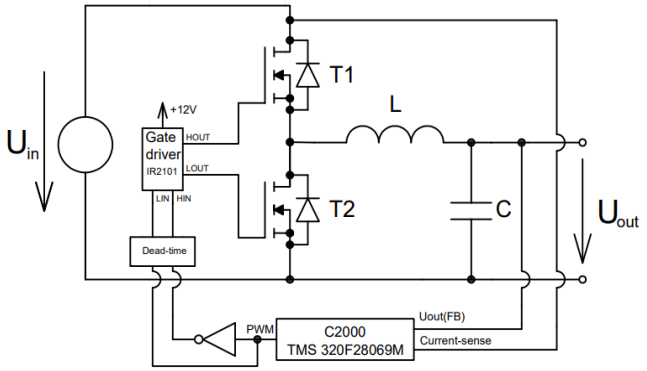

Fig. 14. Circuit diagram of the primary side DC/DC buck converter.

The values of the currents of transistors and capacity of the output capacitor are evaluated using (8)–(10):

$$I_{T_H(AV)} = \frac{1}{T_{SW}} \times \int_0^{t_{on(\max)}} \left(I_{Lpeak(min)} + \frac{I_{Lpeak(max)} - I_{Lpeak(min)}}{t_{on(\max)}} \times t \right) dt =$$

$$= \frac{1}{10,204 \cdot 10^{-6}} \times \int_0^{2,381 \times 10^{-6}} \left(2,429 + \frac{3,286 - 2,429}{2,381 \times 10^{-6}} \times t \right) dt = 0,667 A, \qquad (8)$$

$$I_{T_L(AV)} = \frac{1}{T_{SW}} \times \int_0^{t_{off}(\max)} \left(I_{Lpeak(\max)} + \frac{I_{Lpeak(min)} - I_{Lpeak(max)}}{t_{off}(\max)} \times t \right) dt =$$

$$= \frac{1}{10,204 \times 10^{-6}} \times \int_0^{7,823 \times 10^{-6}} \left(3,286 + \frac{2,429 - 3,286}{7,823 \times 10^{-6}} \times t \right) dt = 2,19 A, \qquad (9)$$

$$C_{out(min)} = \frac{I_{out} \times D_{\max}}{f_{SW} \times \Delta V_{out}} = \frac{2,857 \times 0,233}{98 \times 10^3 \times 50 \times 10^{-3}} = 136,1 \times 10^{-6} F. \qquad (10)$$

Full-Bridge inverter. The circuit schematic for the considered solution of Full-Bridge Inverter within the proposed e-scooter WChS is shown in Fig. 15. Core controller of this converter is TMS 320F228069M. The optimal transistor was chosen based on a comparison of the Figure of merit (FOM) parameters of three types of transistors. All three compared transistors are of the CoolMOS type. Equation (11) was used to calculate the FOM parameter

$$FOM = R_{DS(on)} \times Q_{GS}. \qquad (11)$$

The main circuit components of full-bridge inverter are listed in Table VIII. Transistor IPP60R360P7 from Infineon was selected due to low values of the internal capacitances and a fast internal diode. Figure 16 shows the experimental model of the full-bridge inverter as an example of one power converter stage of the proposed wireless charging system.

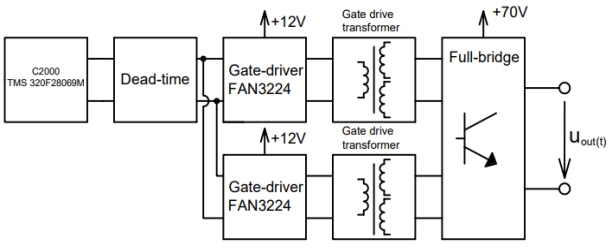

Fig. 15. Circuit diagram primary side inverter.

TABLE VIII. LIST OF USED CIRCUIT COMPONENTS OF THE INVERTER.

Component	Type/SN
Control circuit	TMS320
Power transistor	IPP60R360P7

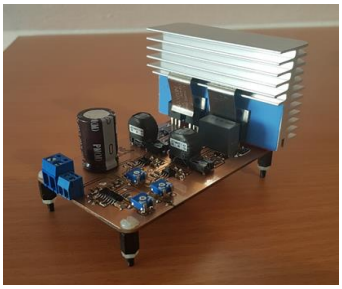

Fig. 16. Experimental model of the full-bridge inverter.

Secondary side rectifier. To rectify the induced voltage on the secondary side, a full-bridge rectifier consisting of Schottky diodes was used. A type MBR40250G diode is used. The value of the filter capacitor was determined according to the relation (12) (Table IX)

$$C = \frac{I_{OUT}}{\omega_0 \times \Delta C_S} = \frac{4,7}{2 \times \pi \times 85000 \times 50 \times 10^{-3}} = 176 \mu F. \qquad (12)$$

TABLE IX. LIST OF USED CIRCUIT COMPONENTS OF THE PROPOSED RECTIFIER.

Component	Type/SN
Schottky diode	MBR4025G
Output capacitor [uF]	220

Secondary side DC/DC buck converter. This converter works in CV/CC mode for optimal charging of the e-scooter battery. The control is provided by a microcontroller TMS 320F28069M.

The value of inductance of the buck converter is given by (13)

$$L = \frac{U_{in(\max)} - U_{OUT}}{\Delta I_L} \times t_{on(\min)} = \\ = \frac{90-42}{1,429} \times 6,122 \times 10^{-6} = 160 \times 10^{-6} H, \quad (13)$$

where ΔI_L is the current ripple of the coil and U_{out} is the output voltage of the buck converter, while $U_{in(max)}$ is the maximal value of the input voltage.

The values of the currents of the transistor, diode and capacity of the output capacitor are evaluated using (14)–(16):

$$I_{T(AV)} = \frac{1}{T_{SW}} \times \int_0^{t_{on(\max)}} \left(I_{Lpeak(\min)} + \frac{I_{Lpeak(\max)} - I_{Lpeak(\min)}}{t_{on(\max)}} \times t \right) dt = \\ = \frac{1}{10,204 \times 10^{-6}} \times \int_0^{8,571 \times 10^{6}} \left(4,048 + \frac{5,476 - 4,048}{8,571 \times 10^{-6}} \times t \right) dt = 4A, \quad (14)$$

$$I_{D(AV)} = \frac{1}{T_{SW}} \times \int_0^{t_{off(\max)}} \left(I_{Lpeak(max)} + \frac{I_{Lpeak(min)} - I_{Lpeak(max)}}{t_{off(max)}} \times t \right) dt = \\ = \frac{1}{10,204 \times 10^{-6}} \times \int_0^{1,633 \times 10^{-6}} \left(5,476 + \frac{4,048 - 5,476}{1,633 \times 10^{-3}} \times t \right) dt = 0,762A, \quad (15)$$

$$C_{out(\min)} = \frac{I_{out} \times D_{\max}}{f_{SW} \times \Delta V_{out}} = \frac{4,762 \times 0,84}{98 \times 10^{3} \times 50 \times 10^{-3}} = 816,3 \times 10^{-6} F. \quad (16)$$

The main circuit components of the secondary side rectifier are listed in Table X.

TABLE X. LIST OF USED CIRCUIT COMPONENTS OF THE PROPOSED BUCK CONVERTER.

Component	Type/SN
Control circuit	TMS320
Power inductor [uH]	160
Power transistor	IPP60R099P7
Power diode	MBR4025G
Output capacitor [uF]	816.3

V. EXPERIMENTAL MODEL VERIFICATION

Within this part, the experimental verification of the proposed concept is being described. To test the operational characteristics of e-scooter WChS, the focus was given on the identification of the efficiency characteristics of the proposed concept together with the gain characteristics of the coupling elements. The variables for which individual dependencies have been realized are the output power, operational frequency, and distance between coupling elements.

The primary side consists of an EMI filter, a rectifier, a DC/DC (Buck) converter for voltage reduction, and an voltage inverter. The secondary side consists of a rectifier, a DC/DC (Buck) converter and an electronic load. Equivalent resistance values were determined analytically according to [14]. The efficiency is then calculated from the values of the input voltage and current measured by the multimeters and from the values of the output voltage and current measured by the oscilloscope placed as shown in Fig. 17. Measuring equipment serving for evaluation of efficiencies is listed in Table XI.

Input voltage and current were measured with Extech EX430A multimeters. The voltage on the electronic load was measured with a differential probe Hameg HZ 115. The output current was measured with a current probe TCPA 300. The values of the output voltage and current were read from a Tektronix MDO 3054 oscilloscope.

TABLE XI. LIST OF USED MEASURING INSTRUMENTS.

Multimeters	Extech EX430A
Oscilloscope	Tektronix MDO 3054
Current probe	TCPA 300
Voltage differential probe	Hameg HZ 115

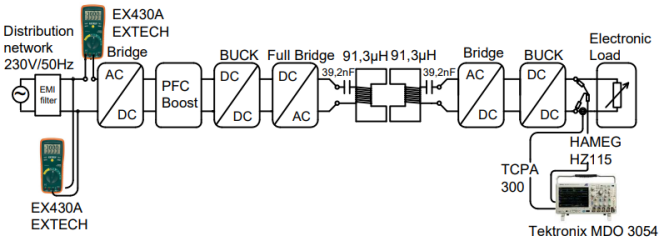

Fig. 17. Laboratory measurement schematic.

A. Measurement of Efficiency Performance vs. Output Power and Transmitting Distance

The first measurement was performed for a mutual distance of the coupling coils of 70 mm. The resonant frequency of the system at this distance was 83.1 kHz. The highest efficiency achieved for a given distance was 80 % for the output power of approximately 100 W. Second measurement was performed for 60 mm of distance between the coupling coils. The resonant frequency was 80.4 kHz, while the highest efficiency achieved was 81.03 % at an output power of approximately 125 W. Last measurements of efficiency performance were realized for 50 mm distance between the coupling coils. The resonant frequency for this case was 96.2 kHz, the highest efficiency achieved was 92.5 % at an output power of 160 W. The graphical interpretation of the previously described results is shown in Fig. 18.

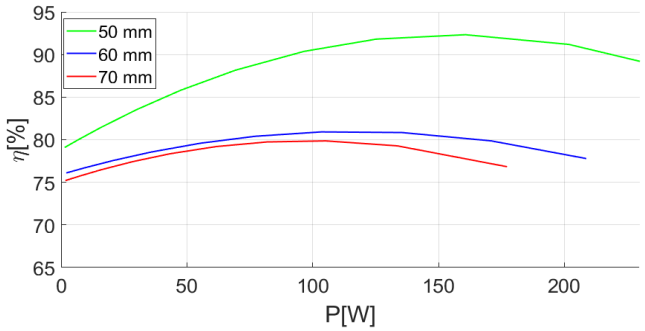

Fig. 18. Efficiency performance vs. output power and transmitting distance.

B. *Measurement of Efficiency and Voltage Gain Characteristic*

In the second part of the laboratory measurements, the focus was given on the investigation of the efficiency and voltage gain characteristics dependent on the operational frequencies. The measurement was performed for a total of sixteen switching frequencies, i.e., within the range from 70 kHz to 105 kHz. At each set of switching frequency, input-to-output voltage and efficiency have been recorded just for the coupling system, i.e., any power electronic converter has been excluded during measurement.

Figure 19 graphically represents the described situation for three different transmitting distances. These characteristics are valuable when the detection of the operational point where simultaneously the highest power and the highest efficiency can be achieved. The highest efficiency (99.55 %) for the coupling coil system was achieved at a distance of 50 mm and frequency of 95.5 kHz. Simultaneously, at this point, a high voltage gain is achieved. At 60 mm, the maximum efficiency was 85 % at a frequency of 90.1 kHz. The value of voltage gain also reaches its maximum. At 70 mm of distance, the efficiency of 90.9 % was achieved at a frequency of 87.6 kHz; here the voltage gain is not reaching its maximum, but opposed to previous situations, it is a little bit higher, thus enabling to transfer more power, but for the sake of reduced efficiency.

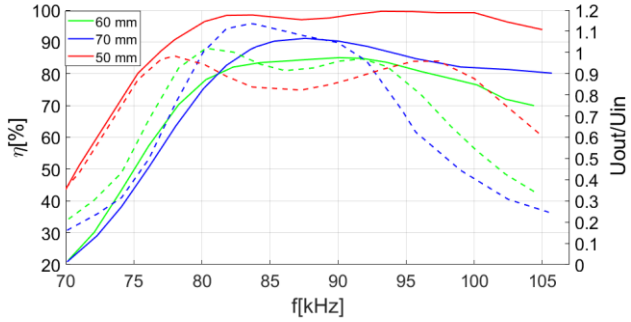

Fig. 19. Comparison of voltage gain profiles and efficiencies of the designed couplers in dependency on operational frequency.

C. *Evaluation of Radiated Magnetic Field of Proposed Coupling System*

With the use of the designed FEM model, the evaluation of the magnetic radiated field according to ICNIRP2010 was realized. The operation was considered for nominal power (200 W), while the distance between coupling coils was set to 50 mm. Figure 20 shows the distribution of the magnetic field within the proposed WChS, whereby the border of the amplitude is set to 27 μT, what is the maximum exposure limit defined by international standards. From the simulation, it is seen that the magnetic induction drops below the limit approximately 0.2 m from the system of coils within the radial or axial direction.

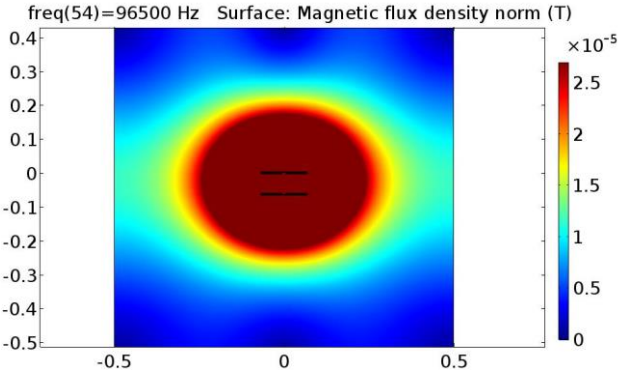

Fig. 20. Magnetic field distribution of the proposed e-scooter WChS at nominal transmitted power and distance of 50 mm between coils.

VI. CONCLUSIONS

The article deals with the possibilities of implementing a contactless charging system for e-scooters, using the known knowledge about the contactless transmission of electricity. In the introduction, it deals with the increase in the use of electric bicycles and e-scooters in road traffic and describes the benefits that contactless charging can bring in this area. In the second part, the article defines the target application area for which the contactless system will be designed and investigates the nominal parameters of chargers designed for electric scooters. In the next part, variants of the arrangement of topologies of power electronic circuits are compared. At the end of the analytical part, the article describes the design and simulation of a model of coupling coils and compensation capacitors. It also simulates the importance of the use of ferromagnetic shielding of coupling coils in terms of compliance with hygiene standards for contactless power transmission. The third part of the article discusses the practical implementation of a real model of the WPT system, including the construction of coupling coils, compensation capacitors, step-down DC/DC converter 400/70 V and a voltage inverter, with the possibility of setting the switching frequency. In the fourth part, the article describes the verification of the functionality of the experimental model of coupling circuits together with the voltage inverter. By means of laboratory measurements, the article investigates the dependences of efficiency on the magnitude of transmitted power for three different mutual distances of coupling coils and the transmission frequency characteristic for these three distances.

CONFLICTS OF INTEREST

The authors declare that they have no conflicts of interest.

REFERENCES

[1] V. Kindl, R. Pechanek, M. Zavrel, and T. Kavalir, "Inductive coupling system for E-bike wireless charging", in *Proc. of 2018 ELECTRO*, 2018, pp. 1–4. DOI: 10.1109/ELEKTRO.2018.8398268.

[2] Michal Frívaldský and Miroslav Pavelek, "In loop design of the coils and the electromagnetic shielding elements for the wireless charging systems", *Energies*, vol. 13, no. 24, p. 6661, 2020. DOI:

10.3390/en13246661.

[3] F. Pellitteri, A. O. Di Tommaso, and R. Miceli, "Investigation of inductive coupling solutions for E-bike wireless charging", in *Proc. of 2015 50th International Universities Power Engineering Conference (UPEC)*, Stoke on Trent, UK, 2015, pp. 1–6. DOI: 10.1109/UPEC.2015.7339964.

[4] F. Pellitteri, V. Boscaino, A. O. Di Tommaso, R. Miceli, and G. Capponi, "Wireless battery charging: E-bike application", in *Proc. of 2013 International Conference on Renewable Energy Research and Applications (ICRERA)*, Madrid, Spain, 2013, pp. 247–251. DOI: 10.1109/ICRERA.2013.6749760.

[5] S.-M. Kim, S.-W. Kim, Jung-Ick Moon, and In-Kui Cho, "A 100W wireless charging system with a human protection function from EM field exposure", in *Proc. of 2016 IEEE Transportation Electrification Conference and Expo, Asia-Pacific (ITEC Asia-Pacific)*, Busan, Korea (South), 2016, pp. 684–688. DOI: 10.1109/ITEC-AP.2016.7513040.

[6] F. Pellitteri, V. Boscaino, A. O. Di Tommaso, F. Genduso, and R. Miceli, "E-bike battery charging: Methods and circuits", in *Proc. of 2013 International Conference on Clean Electrical Power (ICCEP)*, Alghero, Italy, 2013, pp. 107–114. DOI: 10.1109/ICCEP.2013.6586975.

[7] Y. Nagatsuka, N. Ehara, Y. Kaneko, S. Abe, and T. Yasuda, "Compact contactless power transfer system for electric vehicles", in *Proc. of The 2010 International Power Electronics Conference - ECCE ASIA -*, Sapporo, Japan, 2010, pp. 807–813. DOI: 10.1109/IPEC.2010.5543313.

[8] J. Sallan, J. L. Villa, A. Llombart, and J. F. Sanz, "Optimal design of ICPT systems applied to electric vehicle battery charge", *IEEE Transactions on Industrial Electronics*, vol. 56, no. 6, pp. 2140–2149, Jun. 2009. DOI: 10.1109/TIE.2009.2015359.

[9] X.-T. Li, H.-j. Kuang, and L. Zulati, "A research on the operational characteristics of WPT considering reliability limitation", in *Proc. of 2013 International Conference on Advanced Mechatronic Systems*, Luoyang, China, 2013, pp. 213–218. DOI: 10.1109/ICAMechS.2013.6681780.

[10] J. Zhao, T. Cai, S. Duan, H. Feng, C. Chen, and X. Zhang, "A general design method of primary compensation network for dynamic WPT system maintaining stable transmission power", *IEEE Transactions on Power Electronics*, vol. 31, no. 12, pp. 8343–8358, Dec. 2016. DOI: 10.1109/TPEL.2016.2516023.

[11] M. E. Baghdadi, Y. Benomar, O. Hegazy, Y. Yang, and J. Van Mierlo, "Design approach and interoperability analysis of wireless power transfer systems for vehicular applications", in *Proc. of 2016 18th European Conference on Power Electronics and Applications (EPE'16 ECCE Europe)*, Karlsruhe, Germany, 2016, pp. 1–11. DOI: 10.1109/EPE.2016.7695695.

[12] W. Zhang and C. C. Mi, "Compensation topologies of high-power wireless power transfer systems", *IEEE Transactions on Vehicular Technology*, vol. 65, no. 6, pp. 4768–4778, Jun. 2016. DOI: 10.1109/TVT.2015.2454292.

[13] Y. Wang, Y. Yao, X. Liu, D. Xu, and L. Cai, "An LC/S compensation topology and coil design technique for wireless power transfer", *IEEE Transactions on Power Electronics*, vol. 33, no. 3, pp. 2007–2025, Mar. 2018. DOI: 10.1109/TPEL.2017.2698002.

[14] V. Kindl and M. Frívaldský, M. Zavrel, and M. Pavelek, "Generalized design approach on industrial wireless chargers", *Energies*, vol. 13, no. 11, p. 2697, 2020. DOI: 10.3390/en13112697.